Are flow-vegetation interactions well represented by mimics?

A case study of mangrove pneumatophores

- *Revised manuscript*

E. M. Horstman[1*], K. R. Bryan[1], J. C. Mullarney[1], C. A. Pilditch[1], C. A. Eager[1]

[1]Coastal Marine Group, Faculty of Science and Engineering, The University of Waikato, Private Bag 3105, Hamilton 3240, New Zealand

*Corresponding author: erik.horstman@waikato.ac.nz

Keywords: vegetated flow; *Avicennia marina*; mangrove pneumatophores; vegetation mimics; turbulence

Highlights (85 characters each)

- ~~Real pneumatophores exhibit heterogeneity in shape, height and spatial distribution~~
- Vegetation heterogeneity has minor effects on relative within-canopy velocities
- Discrete canopy density transitions do intensify and confine the canopy shear layer
- Uniform-height canopies ~~dowels generate stronger~~ enhance turbulence maxima and within-canopy turbulence~~than variable-height canopies~~
- Bed shear stress in pneumatophores two times smaller than in uniform-height dowels

Formatted: Font: Bold, Complex Script Font: Bold

Abstract

Arrays of real mangrove pneumatophores and artificial dowel mimics were constructed in a laboratory flume to compare differences in flow dynamics. Compared to the uniform-height dowel canopy, the non-uniform height of the pneumatophores significantly reduced the intensity of the canopy shear layer, and shifted the turbulence maxima from directly above the dowels upwards by approximately the standard deviation of the pneumatophore heights. Consequently, bed shear stresses were up to two times greater in the uniform-height dowel canopy than in a pneumatophore canopy of similar density. At the same time, ratios of the within-canopy velocity to the free-stream velocity above the canopies were not significantly altered by heterogeneous heights, shapes and spatial distributions of the pneumatophores. Our results emphasize that uniform dowels are poor proxies of real pneumatophore canopies and may lead to underestimates of sediment-trapping efficiency.

1 Introduction

Aquatic vegetation imposes a significant drag force on the surrounding water, altering flow velocity, turbulence and transport of suspended matter. Consequently, water motions through vegetation canopies, such as mangrove root systems and saltmarsh grasses, have been widely studied [reviewed by e.g. 1, 2-4]. While the vegetative drag tends to reduce horizontal current velocities within the vegetation, continuity requires enhanced flow above (or around) the vegetation, leading to increased velocity gradients over the canopy [2, 5, 6]. Resulting velocity gradients at the interface of the canopy and the free-flowing water give rise to large-scale turbulent motions, increasing the exchange of water and suspended matter between the canopy and the water body [7-9].

Elevated turbulence levels over vegetation canopies are able to sustain enhanced concentrations of suspended matter, however, these suspended materials may settle once transported into the less dynamic zone within the vegetation. Consequently, enhanced sediment deposition is often observed within (tidally) submerged canopies of mangrove roots, saltmarsh grasses and seagrass [10-14]. The actual deposition is highly dependent on vegetation properties, sediment supply and characteristics, as well as local hydrodynamic conditions. For example, while Young & Harvey [15] observed a positive correlation between accretion rates and root densities in mangroves, erosion has also been observed in mangroves with relatively high root densities [16-18]. This contrast in accretionary trends in mangroves is directly related to a balance between energy dissipation due to enhanced drag forces and turbulence generation around these root systems [e.g. 19].

An abundance of data on drag and turbulence within aquatic vegetation exists, mostly from experiments with uniform, rigid cylindrical dowels as vegetation mimics, positioned in

random, staggered or aligned arrangements [20-26]. In uniform emergent vegetation, flow speeds within the vegetation monotonically decrease with the vegetation density (measured by $a = Nd$, wherein a is the frontal vegetation cover per unit area [m^{-1}], N is the number of stems per unit area [m^{-2}] and d the stem diameter [m]), the water depth-to-stem diameter ratio (h/d) and the drag coefficient (C_D) induced by the surface roughness of the vegetation elements [21, 27]. Both current velocities and turbulence intensity, expressed as the square-root of the turbulent kinetic energy (k) divided by the flow velocity (u), are found to be approximately constant over the water depth within the emergent canopy, with exception of the near-bed region where peaks have been observed in both velocity and turbulence intensity [6, 21, 27]. While turbulence intensity increases with the presence of sparse emergent vegetation, there exists a critical vegetation density, beyond which the turbulence decreases owing to the reduction in flow speeds occurring at higher densities [27].

Similar to the emergent scenario, in submerged canopies of uniform vegetation elements with height h_c, within-canopy velocities tend to be constant with depth, provided the canopy density is sufficiently large to create a drag force that exceeds the bed stress, which occurs at $ah_c \tilde{>} 0.23$ [2, 28]. Above such a dense submerged canopy, a characteristic logarithmic velocity profile develops for submergence ratios $h/h_c > 1.25$ [21, 29], with an inflection point of the velocity profile near the top of the canopy. Kelvin-Helmholtz instability in this canopy shear layer can give rise to the production of coherent vortices, forming a dynamic mixing layer and causing a local peak in the turbulence profile [20, 21, 30, 31]. The elevation of the logarithmic velocity profile with respect to the top of the submerged canopy, and consequently the penetration depth of the turbulence into the vegetation, depends on vegetation density, the submergence ratio and the vegetation surface roughness [21, 22, 29].

In addition to the above studies that considered idealized artificial canopies, some studies have also used real canopies with heterogeneous properties, both in the field and in the flume [32-34]. However, studies in real canopies often suffer from an inability to comprehensively resolve the hydrodynamics within the irregular (and dynamic) vegetation. This difficulty in obtaining high-resolution data means that the effects of non-homogeneous vegetation properties on the hydrodynamics remain largely unquantified. Liu et al. [35] showed that turbulence production was different in a heterogeneous canopy by studying flow patterns within a double-layer of idealized rigid vegetation. Throughout their experiments, the canopy consisted of various densities of regularly-spaced short and tall acrylic dowels. For sufficiently dense dowel configurations and sufficiently large relative height differences between the short and tall dowels, the velocity and turbulence profiles in the composite canopies resembled a superposition of the profiles for single-layer submerged canopies. However, the shear across the top of each of the vegetation layers was reduced compared to the shear at the top of a uniform-height dowel canopy of the same density, lowering the maximum turbulence production.

These previous studies have highlighted the key principles of hydrodynamics in simplified uniform-height and composite double-layer vegetation canopy mimics. Mangrove pneumatophores are woody aerial roots growing upward from shallow lateral root systems of e.g. *Avicennia* and *Sonneratia* species, reaching heights ranging from a few centimetres to decimetres [36]. These pneumatophores show a considerable resemblance to the rigid cylindrical dowels frequently used as vegetation mimics. However, pneumatophore heights and diameters can vary substantially within the same field site [e.g. 37, 38]. The impacts of such heterogeneity in vegetation characteristics has not been addressed in previous studies.

In a pilot study, we demonstrated that real pneumatophores may have a different effect on the flow dynamics when compared to published studies using dowel mimics [39]. However, the range of experimental conditions used in the published studies made it difficult to isolate and quantify differences. Here, we use dowel canopies that have been designed to mimic the real pneumatophores, allowing for a direct comparison of the flow dynamics in three resembling vegetation canopies: real *Avicennia* pneumatophores (with three different densities), wooden dowels with a variable canopy height equal to the pneumatophores, and wooden dowels of a uniform height. Through these experiments, we explore: (i) the differences in flow dynamics between submerged canopies of real, heterogeneous pneumatophores and idealized dowel canopies of both uniform and variable height; and (ii) the hydrodynamic impacts of density variations in submerged canopies of real pneumatophores, compared to previous results for mimic canopies consisting of uniform dowels. These results provide an evaluation of common practices in physical and numerical modelling that mimic natural vegetation by uniform canopies and the observed differences will be used to identify potential avenues to incorporate effects of the non-uniformity of natural vegetation in such models.

Commented [EH1]: Modified to reflect new focus

2 Methods

2.1 Experimental set-up

Experiments were conducted in a 6.6 m long and 0.5 m wide recirculating acrylic flume with a horizontal bottom [see 40]. The potential gradient across the flume was associated with a water surface gradient only and a steady flow was generated by a variable-frequency impeller that was mounted in the recirculating duct of the flume (Figure 1a). An insert of 0.3 m long stacked 20 mm diameter PVC tubes was used to damp turbulence and rectify unidirectional flow at the entrance of the flume.

Commented [EH2]: As requested by reviewer 2. Should I also include that hence 'the potential gradient was associated with water surface gradient only'? We don't do anything with these gradients later on, so I reckon we could skip this bit.

Vegetation canopies were mounted in large sheets of floral foam that were incorporated in the false floor of the flume, providing a smooth bed over the full flume length. The canopies were 4.0 m long, starting from 0.45 m downstream of the flow rectifier and extended across the full width of the flume (Figure 1a). All data were collected along a series of six cross-sections between 3.0 m and 3.5 m downstream of the leading edge of the canopies (Figure 1a) and flow velocities prior to the implementation of the canopies were obtained from ten spatially averaged observations of the free-stream velocity at either end of the data acquisition area (see section 2.4 for data processing procedures).

Experiments were run with freshwater at three different water depths: 0.12 m, 0.21 m and 0.30 m, mimicking various tidal inundation stages of the canopies. At each water depth experiments were run for two flow rates equating to free-stream flow velocities of 0.10 m/s and 0.15 m/s prior to the implementation of the canopies. Impeller frequencies of the pump were not modified after the introduction of the canopies, in order to maintain a constant flow forcing throughout experiments with the same water depth and flow rate. These experimental conditions are representative of the tidal dynamics in sheltered intertidal mangrove fringes [e.g. 41, 42].

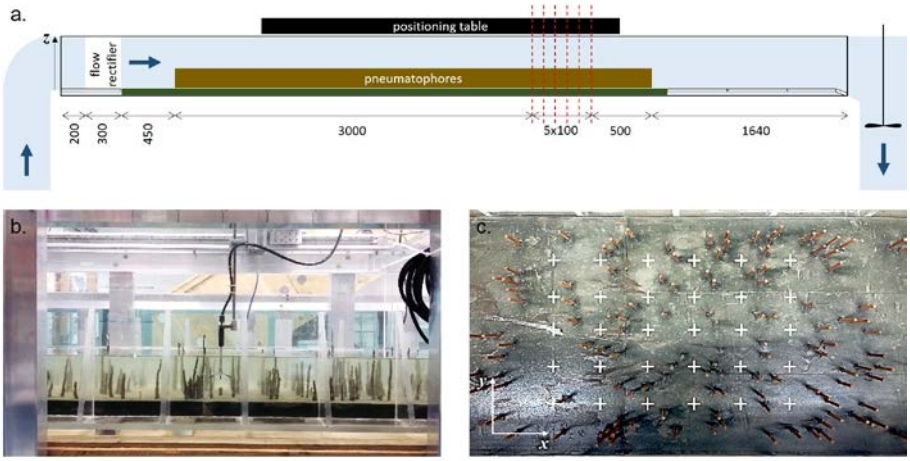

Figure 1 – Experimental setup: (a) Side view of the flume (dimensions in mm) including the vegetation canopy, (b) side view of the data collection area in the flume for the high-density pneumatophore experiment (h = 0.12 m), and (c) top-view of the data collection area for the experiment with uniform-height dowels. Locations for collecting vertical velocity profiles are marked with dashed lines in (a) and white '+'s in (c).

2.2 Vegetation canopies

Experiments were undertaken for a plane bed and for five different canopies: three different densities of real pneumatophores and two high-density dowel canopies with variable and uniform heights (Table 1). Pneumatophores were harvested from the Waikareao Estuary in Tauranga Harbour, New Zealand. In order to obtain a natural spread of the pneumatophores in the flume, scaled photographs of 1x4 m^2 patches of sparse, average and dense pneumatophore covers were collected at the field site prior to harvesting (Figure 2a). These surveys revealed a patchiness of the pneumatophores that was reconstructed in the flume by applying a 0.10x0.10 m^2 raster overlay on both the photo reconstruction and the flume bed (Figure 2b,c).

Commented [EH3]: New section (was part of section 2.1 before)

Formatted: Heading 2

The reconstructed pneumatophore canopies had low (Pneum-LD), average (Pneum-AD) and high (Pneum-HD) densities N of 71, 154 and 268 m^{-2}, respectively. The pneumatophores generally featured a tapered shape with an average basal diameter of 8.1 mm, decreasing to 6.6 mm at mid-height and 4.0 mm at the tip of the pneumatophore, with a depth-mean diameter d of 6.2 mm. The mean pneumatophore diameter remained constant in all three reconstructions (Table 1). The resulting mean cross-sectional pneumatophore density $\varphi = N\pi d^2/4$ ranged from 0.0023 to 0.0086 and the frontal canopy cover per unit area (a) ranged from 0.44 m^{-1} to 1.67 m^{-1} for the low and high pneumatophore densities, respectively (Table 1). These densities were similar to values observed in lower latitude mangrove systems [16, 37, 38].

The average pneumatophore heights h_c differed slightly between densities and across the different experiments the ratio of the water depth to the mean canopy height (h/h_c) ranged from 1.9 to 4.7 (Table 2). Owing to the variability in heights of individual elements (standard deviations of pneumatophore height were up to just over half of the mean canopy height; Table 1), not every pneumatophore was fully submerged for the lowest water depth. Throughout the experiments the pneumatophores behaved as rigid structures that did not move or bend due to the hydraulic forcing, which is similar to their static behaviour in the field when exposed to tidal currents only (personal observation).

Commented [EH4]: Rigid pneumatophores

The high density experiments were reproduced with rigid dowel mimics. Firstly, each pneumatophore was replaced with a dowel of the same height (Figure 2d), resulting in a variable-height dowel canopy (DowVar) with the same horizontal distribution as the pneumatophores (Table 1). Secondly, all dowels were replaced with dowels of a uniform height (DowUni) equal to the mean height of the high-density pneumatophore and variable-

Commented [EH5]: Rigid dowels

height dowel canopies. The cross-sectional density φ for both dowel canopies was slightly smaller than for the high-density pneumatophore canopy owing to the marginally smaller mean diameter of the dowels relative to the pneumatophores (Table 1).

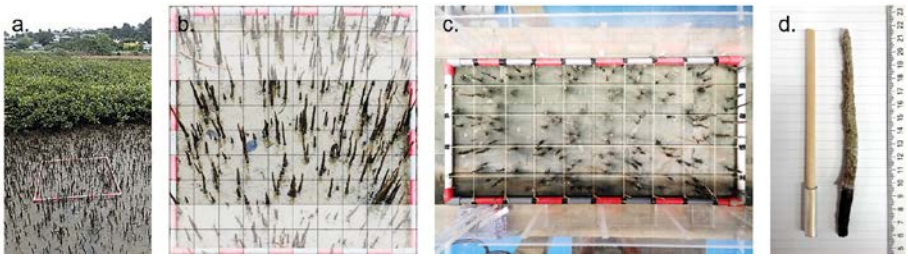

Figure 2 – Canopy reconstruction in the flume: (a) high-density pneumatophore cover in the Waikareao Estuary in New Zealand, (b) a section of the rectified photo resulting from the field survey, ~~and~~ (c) reconstructed canopy in the flume and (d) pneumatophore with a dowel mimic of equal height (the black part of the pneumatophore and the tubed part of the dowel were fixed in the bed).

Table 1 – Vegetation properties of the experiments: heights h_c (mean ±SD of all pneumatophores); diameters d are averages of the top, middle and bottom diameter of each pneumatophore (mean ±SD of >100 pneumatophores); frontal canopy cover per unit area a; and cross-sectional pneumatophore densities φ (as per definition computed with the root-mean-squared pneumatophore diameter).

	Pneumatophores			Dowels	
	low density Pneum-LD	**average density Pneum-AD**	**high density Pneum-HD**	**variable height DowVar**	**uniform height DowUni**
N [m^{-2}]	71	154	268	268	268
h_c [mm]	64 ±25	65 ±34	71 ±38	71 ±38	71 ±0
d [mm]	6.2 ±1.4	6.2 ±1.4	6.2 ±1.4	6.0 ±0	6.0 ±0
a [m^{-1}]	0.44	0.96	1.67	1.61	1.61
φ [-]	0.0023	0.0049	0.0086	0.0076	0.0076

~~2.2~~2.3 Data collection

For each of the canopies, experiments were run at the three different water depths and two flow rates (experimental conditions summarized in Table 2). A fully automated 3D

positioning table (Animatics SmartMotors) allowed for precise positioning and accurate repetitions of hydrodynamic measurements (Figure 1a). Flow and turbulence data were collected with a 10 MHz Nortek Vectrino Profiler (VP) that was mounted on the positioning table (Figure 1b). The VP collected velocity profiles comprising 35 vertical cells of 1 mm each, starting at 40 mm below the probe. Data were collected at a sampling rate of 50 Hz for 60 s at any position (tests conducted with a range of time windows showed that 60 s was long enough to obtain consistent flow characteristics). The VP was moved along the vertical (*z*-direction) to obtain semi-continuous vertical velocity profiles over the full water depths. To account for the inhomogeneity of the velocity field both inside and above the canopy, these vertical velocity profiles were collected at 30 positions within the data collection area (Figure 1a), covering 6 transects with a 100 mm interval in the streamwise *x*-direction and 5 positions with a 75 mm spacing in the lateral *y*-direction along every transect (Figure 1c). The observations were located no less than 0.10 m away from the flume walls to prevent shear from the side walls impacting the measurements. For the plane bed experiments, the streamwise spacing was increased to 500 mm and 10 vertical velocity profiles were collected within the data collection area in order to account for minor streamwise and lateral velocity variations due to imperfections in the flume.

Table 2 – Experimental conditions: Canopy types as in Table 1; water depth h; free-stream velocity U for the plane bed scenario at the same water depth and flow rate (low or high) prior to inserting vegetation; canopy submergence h/h_c; free-stream velocities U_∞ at 0.05 m below the water surface (for experiments with 0.12 m water depth these observations coincided with the top of the canopies, hence no free-stream velocity could be resolved); depth-averaged within-canopy velocities U_c for $0 \leqslant z \leqslant h_c$ and the equivalent depth-averaged velocities U_0 for the plane bed experiments (presented values for U_0 for h_c = 71 mm); ratios of within-canopy velocity to free-stream velocity U_c/U_∞; spatially averaged near-bed

Commented [EH6]: Leaving out Uinf for the 12 cm water depths as requested by reviewer 2.

240 *($z=0.2h_c$) Reynolds stresses $\langle \overline{u'w'} \rangle$; the flow Reynolds number R; the stem Reynolds number of the vegetation Re_d; and the*

241 *estimated drag coefficients C_D of the vegetation elements.*

Canopy type	h [m]	U [m/s]	h/h_c [-]	U_∞ [m/s]	$U_c(U_0)$ [m/s]	U_c/U_∞ [m/s]	$\langle \overline{u'w'} \rangle_{z=0.2h_c}$ [x10^{-5} m^2/s^2]	Re [x10^4]	Re_d [-]	C_D [-]
PlaneBed	0.12	0.10	-	0.10	0.08	-	-1.70	1.09	-	-
PlaneBed	0.12	0.15	-	0.15	0.12	-	-3.54	1.65	-	-
PlaneBed	0.21	0.10	-	0.10	0.07	-	-1.33	1.88	-	-
PlaneBed	0.21	0.15	-	0.15	0.11	-	-3.15	2.85	-	-
PlaneBed	0.30	0.10	-	0.10	0.07	-	-1.23	2.65	-	-
PlaneBed	0.30	0.15	-	0.15	0.10	-	-2.52	3.97	-	-
Pneum-LD	0.12	0.10	1.9	~~0.09~~n.a.	0.07	~~0.78~~n.a.	-1.05	0.98	425	0.7
Pneum-LD	0.12	0.15	1.9	n.a.~~0.13~~	0.10	n.a.~~0.77~~	-2.23	1.47	632	0.7
Pneum-LD	0.21	0.10	3.3	0.11	0.06	0.52	-0.92	1.86	354	1.3
Pneum-LD	0.21	0.15	3.3	0.16	0.09	0.52	-1.93	2.76	527	1.2
Pneum-LD	0.30	0.10	4.7	0.11	0.05	0.46	-0.91	2.61	307	1.7
Pneum-LD	0.30	0.15	4.7	0.16	0.08	0.47	-1.88	3.93	468	1.6
Pneum-AD	0.12	0.10	1.8	n.a.~~0.08~~	0.07	n.a.~~0.78~~	-0.98	0.93	405	0.7
Pneum-AD	0.12	0.15	1.8	n.a.~~0.13~~	0.10	n.a.~~0.79~~	-2.10	1.40	612	0.7
Pneum-AD	0.21	0.10	3.2	0.11	0.05	0.46	-0.81	1.78	312	1.3
Pneum-AD	0.21	0.15	3.2	0.16	0.07	0.46	-1.85	2.64	465	1.2
Pneum-AD	0.30	0.10	4.6	0.11	0.04	0.37	-0.71	2.57	260	1.7
Pneum-AD	0.30	0.15	4.6	0.17	0.06	0.37	-1.53	3.86	391	1.6
Pneum-HD	0.12	0.10	1.7	n.a.~~0.07~~	0.06	n.a.~~0.79~~	-0.53	0.80	354	0.8
Pneum-HD	0.12	0.15	1.7	n.a.~~0.10~~	0.08	n.a.~~0.80~~	-1.02	1.17	521	0.9
Pneum-HD	0.21	0.10	3.0	0.11	0.04	0.37	-0.42	1.70	260	1.3
Pneum-HD	0.21	0.15	3.0	0.17	0.06	0.38	-0.97	2.51	385	1.3
Pneum-HD	0.30	0.10	4.2	0.12	0.03	0.27	-0.33	2.53	203	1.7
Pneum-HD	0.30	0.15	4.2	0.18	0.05	0.27	-0.79	3.81	312	1.6
DowVar	0.12	0.10	1.7	n.a.~~0.07~~	0.06	n.a.~~0.80~~	-0.21	0.81	350	0.5
DowVar	0.12	0.15	1.7	n.a.~~0.11~~	0.09	n.a.~~0.80~~	-0.71	1.25	541	0.4
DowVar	0.21	0.10	3.0	0.11	0.04	0.41	-0.25	1.65	263	0.8
DowVar	0.21	0.15	3.0	0.16	0.07	0.42	-0.55	2.48	400	0.7
DowVar	0.30	0.10	4.2	0.12	0.04	0.31	-0.23	2.49	216	1.1
DowVar	0.30	0.15	4.2	0.18	0.06	0.31	-0.55	3.77	330	0.9
DowUni	0.12	0.10	1.7	n.a.~~0.08~~	0.06	n.a.~~0.74~~	-0.86	0.87	342	1.5
DowUni	0.12	0.15	1.7	n.a.~~0.12~~	0.09	n.a.~~0.74~~	-2.06	1.35	532	1.4
DowUni	0.21	0.10	3.0	0.11	0.04	0.39	-1.09	1.73	264	3.0
DowUni	0.21	0.15	3.0	0.17	0.07	0.40	-2.54	2.64	404	2.9
DowUni	0.30	0.10	4.2	0.11	0.04	0.33	-0.92	2.53	227	3.6
DowUni	0.30	0.15	4.2	0.17	0.06	0.34	-1.99	3.84	352	3.5

242

243 ~~2.3~~2.4 Data processing

244 Data were filtered for correlations ≥70 % and signal-to-noise ratios ≥15 dB [cf. 43] and the

245 procedure of Hurther & Lemmin [44] was applied to remove Doppler noise from the

Formatted Table

Commented [EH7]: Removed these values, as requested by reviewer 2, because no observations above canopies at 12 cm water depth.

turbulent velocities by compensating for the covariance between the two vertical velocity signals that were obtained by the VP. Profiles of Doppler noise exhibited a parabolic shape, with a minimum around the 'sweet spot' of the instrument and larger values towards the extremities of the profiles [45]. Doppler noise only affects the turbulence intensities and hence estimates of turbulent kinetic energy. The Reynolds stress, computed with the horizontal and vertical velocities obtained through the same beam pair of the VP, is unaffected by this noise term [44].

Time-averaged ($\bar{u}, \bar{v}, \bar{w}$) and turbulent ($u', v', w'$) velocities were extracted from each pre-processed data record, with *u*, *v* and *w* denoting the streamwise, spanwise and vertical velocity components, respectively. Turbulent kinetic energy $k = \frac{1}{2}(u'^2 + v'^2 + w'^2)$ and Reynolds stress $u'w'$ (i.e. Reynolds shear stress normalized by the density ρ) were computed for each location at every time. Parameters were then time-averaged over the length of the data records (denoted with overbars). Spatial averages (denoted with angle brackets) were obtained by averaging over all 30 separated vertical profiles (Figure 1c), or 10 profiles for the plane bed experiments [cf. 46].

After application of the above filtering procedures, temporally- and spatially-averaged velocity profiles showed a smooth pattern over the water depth. The turbulence profiles, however, still showed substantial variability along the vertical after correction (to a lesser extent also shown in the Reynolds stress profiles; see e.g. Figure 3b,c), even though Brand et al. [45] found that Hurther & Lemmin's noise removal procedure effectively improved VP data accuracy. Consequently, this paper focusses on the point observations of turbulence properties deemed to be most reliable, located in the 'sweet spot' of the VP at 50 mm below

the probe [47], thus reducing data profiles to a discrete series of point observations with a vertical spacing of 45 mm.

The free-stream velocity over the canopy U_∞ was defined as the (horizontally-averaged) velocity observed nearest to the water surface, i.e. at 0.05 m below the water surface accounting for the instrument size and blanking distance. To calculate the depth-averaged velocity within the canopy U_c, the velocity profiles were linearly interpolated across the data gaps in the vertical and averaged over $0 \leq z \leq h_c$, (Table 1). These interpolations were based on the 10 data points around the sweet spots (to avoid outliers impacting the interpolations), while data from the lowest observation towards the bed were all maintained as there was no interpolation possible. The same procedure was applied for the plane bed experiments to obtain the equivalent average velocity U_0 over each of the heights h_c. Additionally, standard logarithmic velocity profiles were fitted to the spatially-averaged velocity data from the plane bed experiments which resulted in a roughness height z_0 of 1.5×10^{-4} m for the foam bed in the flume [see e.g. 48].

Wake structures behind individual canopy elements depend on the stem Reynolds number $\mathrm{Re}_d = U_c d / \nu$, where ν is the kinematic viscosity of water. Nepf [27] defines the transition from a laminar to turbulent flow regime in vegetated flows as $\mathrm{Re}_d \approx 200$. In the present study Re_d varied between 200-650 (Table 2). Hence, all experiments with vegetation were in the turbulent regime. These stem Reynolds numbers were similar to the vegetation Reynolds numbers observed in tidal marshes [27, 49].

The wakes of individual canopy elements will interact at increasing vegetation densities, enhancing local turbulence and reducing the drag coefficient of individual canopy elements

295 [27, 50]. Hence, the drag coefficient (C_D) of canopy elements is a function of local flow
296 conditions within the vegetation canopy and the structural vegetation characteristics: density
297 N and diameter d. Following Tanino & Nepf (2008), the depth-averaged drag coefficient can
298 be determined by balancing the viscous dissipation of turbulent kinetic energy and the work
299 done by form drag within a vegetation canopy, which yields:

$$\frac{\sqrt{\langle \overline{k} \rangle}}{\langle \overline{u} \rangle} = 1.1 \cdot \left[C_D \frac{2\varphi}{(1-\varphi)\pi} \right]^{1/3}, \quad (1)$$

300 noting that in the present study, the average spacing between the pneumatophores or dowels
301 is >2 times their mean diameter across all densities. Drag coefficients for the vegetation
302 canopies could not be resolved directly through the momentum equation as the water level
303 gradient along the flume was too small to be measured accurately in these experiments.
304

305 **3 Experimental results**

306 3.1 Flow dynamics in canopies of real pneumatophores and dowel mimics

307 To examine the changes in flow dynamics arising from the shape variations and roughness of
308 natural pneumatophores, relative to the commonly-used smooth dowel mimics with a
309 constant diameter (Figure 2d), the results from the experiments with the high-density real
310 pneumatophore canopy are compared to the artificial canopies with the variable-height and
311 uniform-height dowel mimics (Table 1).
312

313 Spatially-averaged depth-integrated velocities within the canopy U_c decreased by up to 51%
314 in the pneumatophore canopy compared to the plane bed velocities U_0 which are depth-
315 averaged over the same vertical extent. Compared to the real pneumatophore canopy, U_c
316 increased with 10 % and 17 % for the variable-height and uniform-height dowel canopies,
317 respectively, at h = 0.30 m (Figure 3a). Within-canopy flow velocities were faster for a

reduction of the water depth and hence the submergence h/h_c of the pneumatophore canopy (Figure 3d); a trend that was observed for all canopies and flow rates (Table 2). The ratio U_c/U_0 was inversely correlated with water depth and hence with canopy submergence for all canopies (Figure 4a), as a greater fraction of the flow got forced through the canopy in the shallower flows.

The increase of the within-canopy velocities in both artificial dowel canopies compared to the pneumatophore canopy could be explained by the slightly smaller density of the dowels compared to the pneumatophores, reducing the total canopy resistance (Figure 4a). Although the dowels had an average diameter and density very close to the real pneumatophores (Table 1), the tapered shape of the pneumatophores led to a change in the gradient of the vertical velocity profile. In particular close to the bed, where the real pneumatophores were widest, faster flow speeds were observed in the experiments with the variable-height dowels (Figure 3a).Within the uniform-height dowel canopy, the velocity increase was more pronounced in the region around the top of the dowel canopy (at $z = h_c$) when compared to the high-density pneumatophore canopy. With both dowel canopies having the same density, these differences of within-canopy flow patterns are owing to the varying height structure of the canopies.

Flow velocities above each of the three canopies were higher than those over a plane bed for heights exceeding two times the canopy height ($z \tilde{>} 2h_c$; Figure 3a). In this region, velocities above the variable-height dowel canopy were smaller than the flow velocities over the pneumatophores, due to the fixed flow forcing and the higher within-canopy velocity in the dowels. For the uniform-height dowel canopy, only the free-stream velocities above $z/h_c \approx$ 2.5 were reduced compared to velocities over the pneumatophore canopy.

Distortion of the vertical flow profile due to the canopies was expressed by the ratio of the within-canopy velocity U_c to the free-stream velocity U_∞ [cf. 22, 51]. For the pneumatophore cover, this ratio was 0.27 for h = 0.30 m, whereas for the plane bed the equivalent ratio U_0/U_∞ was 0.67. Compared to the experiments with real pneumatophores, the ratio U_c/U_∞ was 10-15% greater for the variable-height dowels and up to 25% greater for the uniform-height dowels (Table 2). The flow forcing, as imposed by the fixed impeller frequencies for the low and high flow regimes at each water depth, had no effect on the ratio of the flow velocity within the vegetation and the free-stream velocity above the vegetation canopy and U_c/U_∞ was constant across each set of experiments with the same canopy and water depth (Table 2). When normalized by the spatially averaged velocity at the top of the canopy $\langle \overline{u} \rangle_{z=h_c}$ [cf. 23], the velocity profiles for each canopy collapsed for the three water depths and two flow rates (Figure 3g).

The vertical shear at the top of the canopies is associated with the generation of Kelvin-Helmholtz vortices [29]. Consequently, the turbulence and Reynolds stresses peaked around the inflection points of the velocity profiles. Turbulence maxima occurred at $z \approx 1.5h_c$ for the pneumatophores and variable-height dowels (Figure 3b,c), a level that equated to the mean plus one standard deviation height of these canopies (Table 1). However, for the uniform-height dowel canopy, turbulence maxima were observed closer to the canopy at $z \approx h_c$, similar to results from past studies with uniform-height dowels [e.g. 20, 22, 29, 52].

Turbulence was less intense for the experiments with variable-height dowels than with real pneumatophores, but the much greater gradient of the velocity profile at the interface of the uniform-height dowel canopy resulted in a stronger shear-layer with significantly greater vortex-generating capacity (Figure 3b,c). The maximum reduction of turbulence and

368 Reynolds stress in the variable-height dowel canopy compared to the pneumatophores was
369 observed at $z \approx 2.1h_c$ and ranged around 25% and 34%, respectively, for the experiments with
370 0.30 m water depth. Conversely, near the top of the uniform dowel canopy, at $z \approx 0.8h_c$,
371 turbulence increased by about 114% and Reynolds stresses had increased by 228% compared
372 to the pneumatophore canopy. Differences in turbulence and Reynolds stresses right at the
373 top of the dowel canopy may have been even more pronounced, but these could not be
374 resolved from the data (see section 2.3). The enhanced turbulence in the uniform-height
375 dowels was observed throughout the canopy, causing near-bed Reynold's stresses to be of
376 similar magnitude as over the plane bed, whereas both variable height canopies (natural and
377 mimics) caused a much greater attenuation of these stresses (Figure 3c).
378
379 A reduction of the canopy submergence increased the turbulent kinetic energy (Figure 3e)
380 within and just above the canopies [cf.29], owing to the enhanced within-canopy velocities
381 occurring at shallower water depths. Vertical profiles of the turbulence intensity $\sqrt{\langle \overline{k} \rangle} / \langle \overline{u} \rangle$
382 and the normalized Reynolds' stresses $\sqrt{-\langle \overline{u'w'} \rangle} / U_c$ were similar between experiments with
383 different flow rates (Figure 3h,i), but profiles did not collapse for the different water depths
384 (cf. the normalized velocity profiles in Figure 3g). However, the reduction of the near-bed
385 turbulence and Reynolds stress in the variable-height dowels and their increase in the
386 uniform-height dowels, compared to the high-density pneumatophores, was consistent for all
387 water depths and flow regimes (Table 2).
388

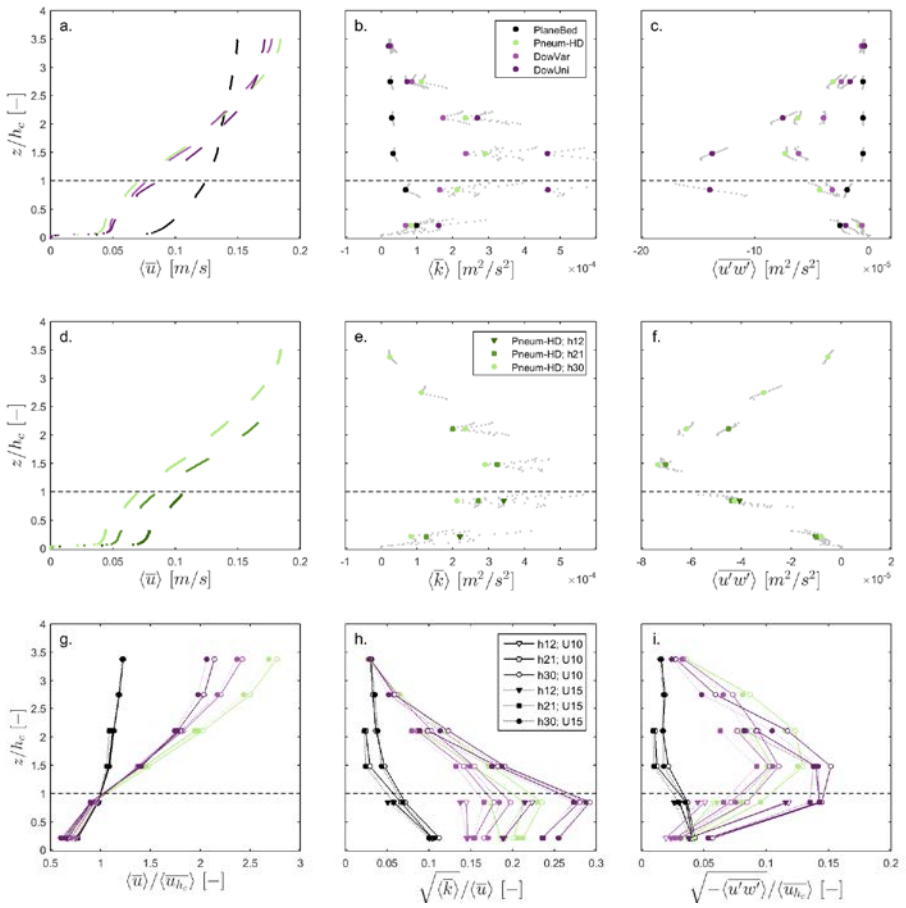

Figure 3 – Combined results of the flume experiments for high-density real and artificial canopies. Spatially-averaged vertical profiles of (a) streamwise velocity, (b) turbulent kinetic energy, and (c) Reynolds stress, for a plane bed, the high-density canopy of real pneumatophores, dowels with variable heights that are similar to the pneumatophore heights, and dowels with a uniform height equal to the average pneumatophore height (see Table 1), all at 0.30 m water depth and for the high flow rate (U = 0.15 m/s). (d-f) Show the same profiles for the pneumatophore canopy as (a-c) but at multiple water depths (and the high flow rate U = 0.15 m/s). Spatially-averaged vertical profiles of (~~d~~g) streamwise velocity scaled by the velocity at the top of the canopy, (~~e~~h) turbulence intensity, and (~~f~~i) friction velocity scaled by the velocity at the top of the canopy, for the different canopies (~~different~~ colours as in a-c) at all water depths (symbols as in d-f) and at both flow rates. Dashed horizontal lines indicate the average canopy height. Panels (b,c,e,f) present the reliable turbulence observations from the sweet spots (solid symbols) and the noise-affected observations for the remainder of the observed profiles (grey

dots; see text for details). Legend key: canopy types as in Table 1; h12/h21/h30 = 0.12/0.21/0.30 m water depth; U10/U15 = low/high flow rate comparing to a free-stream velocity of 0.10/0.15 m/s over the plane bed.

Drag coefficients for the dowels in the variable-height dowel canopy were 37-51% lower than those computed for the high-density pneumatophores, other conditions kept equal (Table 2), likely owing to the smooth dowel surface compared to the relatively rough surface of the pneumatophores (Figure 2d). Conversely, the computed element drag coefficients for the uniform-height dowels were 3-4 times higher than those obtained for the variable-height dowels, even though the material was the same, and around 2 times higher than those for the real pneumatophores (Table 2). These canopy drag coefficients computed from (1) were mostly unaffected by the flow forcing (Table 2). However, the increasing within-canopy turbulence at shallower water depths resulted in a decrease of the vegetation drag coefficient with a reduction of the canopy submergence.

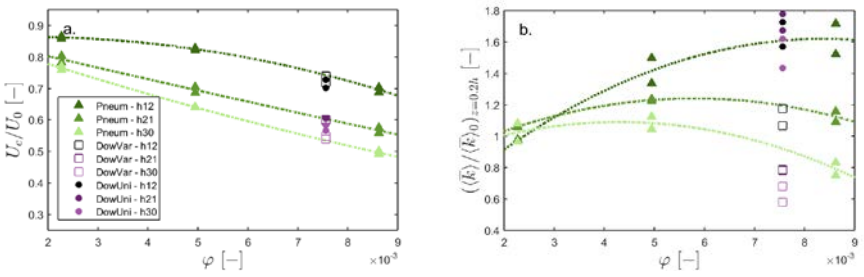

Figure 4 – Comparison of within-canopy flow conditions relative to the no-vegetation case:(a) ratios of the within-canopy velocity to the plane bed velocity ($0<z<h_c$) and (b) ratios of the near-bed turbulent kinetic energy ($z = 0.2h_c$) in vegetated and plane bed (subscript 0) conditions. Dotted lines are fits (cubic spline) illustrating the different trends in the flow dynamics for the real pneumatophores at the various water depths.

3.2 Effects of canopy density in real pneumatophores

Pneumatophore canopies with different densities were used for further comparison of the hydrodynamic behaviour of canopies composed of real pneumatophores versus dowel mimics (results provided in supplementary material). Spatially-averaged depth-integrated velocities within the different pneumatophore canopies U_c decreased by up to about 24%, 36% and 50% compared to the plane bed velocities U_0, for the low, average and high pneumatophore densities, respectively (Figure 4a). Near-bed turbulence was largest for the average canopy density, with lower values observed in both the sparse and dense pneumatophore canopies (Figure 4b). A similar dependency of turbulence on canopy density was found in flume experiments with submerged bamboo vegetation mimics [12] and in a natural stream with submerged and emergent macrophytes [53]. These results of the pneumatophore experiments show evidence of the competing effects of an increasing vegetation density, causing the flow to slow down while at the same time facilitating greater wake production [27]. The computed drag coefficients for the pneumatophores were largely independent of the canopy density and the imposed flow forcing and reduced from 1.7 to 1.3 and to 0.8 for water depths of 0.30, 0.21 and 0.12 m, respectively.

Depth-averaged within-canopy velocities decreased monotonically with increasing vegetation densities across all experiments (Figure 4a). To enable the comparison of the results over the full range of experiments, we defined an adjusted vegetation density that is the product of the vegetation density φ and the submergence ratio h/h_c. The within-canopy velocities relative to the plane bed velocities (U_c/U_0), demonstrated a significant and negative correlation (r = -0.98, $p \ll 0.01$) with this submergence-adjusted density parameter $\varphi(h/h_c)$ across all experiments with pneumatophores (Figure 5a). This relationship is a result of the fact that both larger vegetation densities and larger submergence ratios led to a decrease in within-

canopy flow speeds (Figure 4a). The same submergence-adjusted density parameter also showed a significant but positive correlation (r = 0.92, $p \ll 0.01$) with the near-bed turbulence intensities in the pneumatophore canopies (Figure 5b).

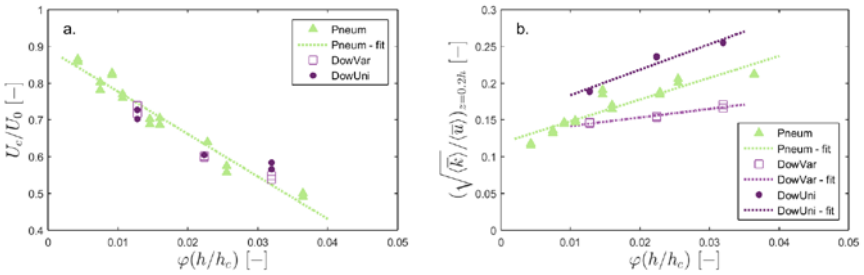

Figure 5 – Correlations of the relative within-canopy flow conditions with the submergence-adjusted vegetation densities: (a) the ratios of the within-canopy velocities to the near-bed velocities over a plane bed (U_c/U_0) correlate significantly with the density parameter $\varphi(h/h_c)$ for the pneumatophore data (r = -0.98, $p \ll 0.01$) and (b) the near-bed turbulence intensity, at z = 0.2h, correlates positively with the submergence-adjusted vegetation density in each of the different canopies with r = 0.92, 0.97 and 0.97 ($p \ll 0.01$) for the experiments with pneumatophores (Pneum), variable-height dowels (DowVar) and uniform-height dowels (DowUni), respectively.

4 Discussion

The variable shape and height of the pneumatophores was found to have no substantial impact on the attenuation of the within-canopy velocity in comparison to the canopies of dowel mimics, as the results for the dowel experiments collapse well onto the obtained relationship between the submergence-adjusted vegetation density and the velocity attenuation U_c/U_0 (Figure 5a). This result is confirmed by a comprehensive comparison with data from prior studies using uniform-height dowels [20, 22-24, 51]. These data cover 62 experiments and encompass a wide range of canopy densities and submergence ratios and demonstrate a significant and negative correlation between the calculated (or estimated)

ratios of the within-canopy velocity to the free-stream velocity above the vegetation (U_c/U_∞) and the submergence-adjusted vegetation density (Figure 6a). In general, the ratios U_c/U_∞ from the present experiments are in good agreement with the data obtained from the past experiments with uniform-height dowels. In both the present and previous studies, an increasing density, an increasing submergence ratio of the canopy, or a combination thereof, resulted in a non-linear decrease of the ratio U_c/U_∞, expressed by the fitted power law $U_c/U_\infty = 0.13(\varphi(h/h_c))^{-0.30}$ ($R^2 = 0.72$). Given the similarity of the ratios of the within-canopy velocity to the free-stream velocity in the pneumatophore canopies with those observed in uniform-height dowel canopies in the present and past studies, it can be concluded that the variable shape and height of the pneumatophores in this study does not result in a significantly different vertical distribution of the streamwise velocities than the idealized uniform-height dowels.

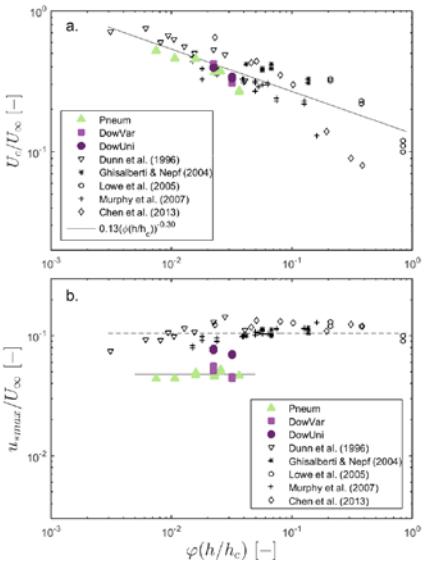

Figure 6 – Data from the present work in comparison to data compiled from previous studies in artificial canopies of uniform-height dowels (experiments with 0.12 m water depth were omitted from this analysis as U_∞ was unresolved). (a)

Commented [EH8]: Removed 12 cm water depth data

Ratios of the within-canopy velocity to the free-stream velocity were found to correlate significantly ($r=-0.64$, $p<<0.01$) with the submergence-adjusted canopy density $\varphi(h/h_c)$. The solid line presents a power law fit for the results of both present and previous studies ($R^2 = 0.76$). (b) The maximum friction velocity scaled by the free-stream velocity varied around a constant value of 0.048 (SD = 0.004) for the experiments with pneumatophores and variable-height dowels (solid line), which is significantly lower (one-sided t-test, 95% confidence level, $p<<0.01$) than the average of 0.105 (SD = 0.016) throughout the present and previous results for uniform-height dowels (dashed line).

The observed unique relationship between the velocity reduction and the submergence-adjusted vegetation density emphasizes the governing role of the canopy submergence on the dynamics of vegetated flows. All data presented consider shallow submergence ratios ($h/h_c <$ 5) for which the flow within the canopy is determined by the balance between pressure gradients, canopy drag and turbulent stresses [54]. In emergent canopies ($h/h_c \leq 1$), water flow through the canopy is primarily the result of the balance between the pressure gradient and the vegetative drag only, as the contribution by (stem-scale) turbulence often is negligible. For submerged vegetation ($h/h_c > 1$), the shear layer at the top of the vegetation contributes to the turbulent stresses within the vegetation. In a canopy consisting of uniform dowels, the characteristic scale of the shear layer turbulence and, hence, the penetration of turbulent stresses into the vegetation, is limited for submergence ratios $1 < h/h_c < 2$ [29].

The similarity between the experiments with dowels and with pneumatophores did not extend to the turbulence in the canopy shear layer (Figure 5b) and our results showed that the height-variation of the vegetation density had a substantial effect on the turbulence production. The maximum value of the spatially-averaged non-dimensional friction velocity, i.e. $u_{*\max} = \sqrt{-\left\langle \overline{u'w'} \right\rangle_{\max}}$, scaled by the free-stream velocity, was found to be approximately constant over the full range of conditions in both the collection of past experiments and in the present experiments with uniform-height dowels, with a mean value of 0.105 (Figure 6b).

512 This finding was consistent with observations from Lowe et al. [22], who concluded that the
513 non-dimensional canopy-induced friction velocity was about 0.1 throughout their
514 experiments. However, the present experiments with variable-height canopies of
515 pneumatophores and dowels produced significantly lower values (one-sided t-test, 95%
516 confidence level, $p<<0.01$) for this non-dimensional friction velocity, with a mean value of
517 0.048 (Figure 6b).
518
519 The reduction of the maximum friction velocity over the variable-height canopies, even
520 though the vertical distribution of the streamwise velocity profile for these canopies was
521 similar to the uniform-height dowel canopies, can be attributed to changes in the canopy
522 shear layer owing to the gradual decline of the vegetation density along the vertical. The
523 turbulent exchange of momentum at the top of the canopy is controlled by shear-scale
524 vortices, and so the friction velocity at the top of the canopy $u_{*h_c} = \sqrt{-\left\langle \overline{u'w'} \right\rangle_{z=h_c}}$ scales with
525 the velocity gradient across the water column, or the vortex velocity scale, ΔU [28]. Based on
526 a subset of the data collated in Figure 6, Nepf et al. (2007) obtained a positive relationship
527 between the ratio $\Delta U / u_{*h_c}$ and the canopy drag parameter $C_D a h_c$ (Figure 7). This relationship
528 indicates that the exchange of momentum becomes less efficient as the vortex scale decreases
529 for denser canopies, diminishing the Reynolds stress for a given velocity gradient. We
530 computed the same parameters for our experiments (Figure 7), substituting the friction
531 velocity at the top of the canopy with the maximum friction velocity $u_{*\max}$ (where $u_{*\max}$ equals
532 u_{*h_c} for uniform-height canopies), and using $\Delta U = U_\infty - U_c$. The uniform-height dowel
533 experiments of the present study compared well with the relationship derived by Nepf et al.
534 (2007). However, the variable-height canopies produced much higher values for $\Delta U / u_{*\max}$
535 (Figure 7). This difference coincides with the consistently lower values of the normalized

maximum friction velocity in Figure 6b for these canopies, due to its similarity with the inverse of the ratio $\Delta U/u_{*\max}$. The reduced efficiency of the vertical momentum exchange across the pneumatophores and variable-height dowel canopies is associated with the heterogeneity of the canopy height, preventing the formation of a confined canopy shear layer as it is observed in the case of a discrete density transition at the top of uniform-height dowel canopies (Figure 3c; cf. Ghisalberti & Nepf, 2004).

The canopy shear layer is associated with an inflection point in the velocity profile, which was observed in all velocity profiles for the two highest water depths used here (Figure 3g, Figure 9d), similar to the observations of King et al. [5]. The canopy drag parameter for the present experiments was as small as $C_D a h_c = 0.03$, whereas previous studies only identified a well-defined shear layer and inflection point in the velocity profile for $C_D a h_c > 0.1$ [23, 28, 52]. Moreover, previous studies identified velocity inflection points and turbulence maxima at the top of the uniform-height vegetation at $z = h_c$ [e.g. 5, 28], but for the variable-height canopies in the present study inflection points and turbulence maxima were observed at height $z \approx 1.5h_c$, equating to the mean pneumatophore (or dowel) height plus one standard deviation of the height of the canopy elements (Table 1).

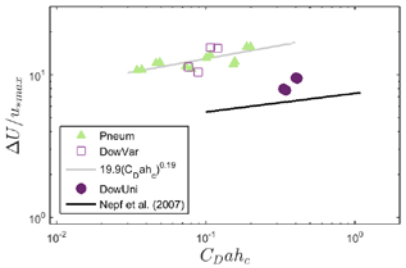

Figure 7 – Comparison of the ratio of the vortex velocity scale ΔU and the maximum friction velocity $u_{*\max}$ for different vegetation types (for uniform-height canopies this maximum occurs at $z \approx h_c$, for variable-height canopies at $z \approx 1.5h_c$). The

black line represents the relationship obtained by Nepf et al. (2007) for uniform-height dowels. The ratios for the pneumatophores and the variable-height dowels also correlate positively with the canopy drag parameter $C_D a h_c$ as indicated by the grey line ($r=0.69$, $p<0.01$), but are substantially higher than those for the uniform-height dowels. (Experiments with 0.12 m water depth were omitted from this analysis as U_∞ was unresolved.)

The spatial distribution of the vegetation elements within canopies was found to have no significant impact on the flow dynamics. All canopies in the present study were based on the natural patchy spatial distribution of the pneumatophores. In Figure 6, the results of the uniform-height dowel experiments from the present study were in good agreement with results from previous studies using random [24, 51] as well as staggered dowel placements [20, 22, 23]. This similarity implies that the non-uniform spatial distribution of the vegetation elements within the canopy is of lesser importance relative to the impact of the non-uniform height of the dowels or pneumatophores.

The results provide evidence that simulations of a natural non-uniform canopy with uniform-height dowel mimics could significantly over-estimate the maximum Reynolds stress in the canopy shear layer and hence its contribution to transport of sediment over and into the vegetation canopy. The canopy shear layer that develops at the top of the submerged canopies enhances turbulent mixing and plays a crucial role in the exchange of both momentum and mass between the canopy and the flow above [8]. The maximum Reynolds stress for the dense pneumatophore canopy in this study was observed to be up to 2.9 times greater than the maximum stress over a plane bed under the same flow conditions (Figure 3c). This result is consistent with observations by Lacy and Wyllie-Echeverria [33] of Reynolds stresses at the top of macro-tidal eelgrass canopies being 2-4 times greater than the maximum stress over the plane sea bed. However, when the pneumatophores were replaced by uniform-height

582 dowels, the maximum stress in the canopy shear layer was up to 5.6 times greater than over
583 the plane bed (Figure 3c).
584
585 Penetration of the turbulence from the canopy shear layer into the vegetation canopy is a key
586 parameter in assessing the influence on sediment entrainment and has been shown to be
587 reduced for high density canopies [55]. We estimated the spatially-averaged bed shear stress
588 from the near-bed Reynolds stress: $\langle \tau_b \rangle = -\rho \langle \overline{u'w'} \rangle_{z=0.2h_c}$ at 0.015 m above the bed ($z = 0.2h_c$).
589 The ratio of the bed shear stresses in the pneumatophore canopies and the bed shear stress
590 over the plane bed $\langle \tau_b \rangle / \tau_{b,0}$ showed a significant negative correlation with the pneumatophore
591 density (Figure 8), irrespective of the level of submergence of the canopy, indicating that
592 erosion potential was reduced for higher pneumatophore densities. Similarly, bed shear
593 stresses in eelgrass beds were observed to be about 5.7 times smaller than at a nearby bare
594 site [56]. The reduction of the bed shear stress to sub-critical values and hence the reduction
595 of sediment transport capacity within (dense) vegetation canopies has been observed to
596 enhance sediment deposition in both rigid and flexible submerged canopies [12, 56, 57].
597
598 Reduced vertical variability of the canopy density within a canopy of variable-height dowels
599 compared to the (tapered) pneumatophores, combined with the smoother surface of the
600 dowels, was found to reduce the near-bed turbulence intensity (Figure 5b), giving rise to a
601 substantial decrease in the erosion potential within the canopies (Figure 8). Compared to the
602 high-density canopy of real pneumatophores, we observed markedly lower near-bed
603 turbulence in the variable-height dowel canopies (Figure 4b) and bed shear stresses were
604 about 2 times lower than the expected value for a real pneumatophore canopy of similar
605 density (Figure 8), even though the scaled maximum friction velocity was similar for those

606 two canopy types (Figure 6b). The lower near-bed turbulence in the variable-height dowels is
607 a combined effect of the impact of the tapered shape of the pneumatophores, enhancing the
608 vertical gradient of the vegetation density, on the within-canopy velocity distribution (Figure
609 3a) and the reduced turbulence production around the smoother surface of the mimics (Figure
610 2d; Figure 3b,c).
611

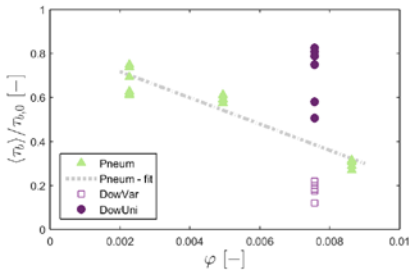

612

613 *Figure 8 – The ratio of the spatially-averaged bed shear stresses in the pneumatophore canopies* $\langle \tau_b \rangle$ *to the bed shear*
614 *stress on the plane bed* $\tau_{b,0}$ *declines significantly at higher pneumatophore densities, as shown by the linear fit (r=-0.95,*
615 *p≪0.01). Bed shear stresses in the artificial dowel canopies do not comply with the relative bed shear stress predicted for a*
616 *pneumatophore cover of the same density, as shown by the fitted line.*

617

618 Variability in the height of the canopy reduced the near-bed turbulence intensity (Figure 5b)
619 and scaled friction velocity (Figure 6b), causing a substantial decrease of the erosion potential
620 in such canopies compared to a uniform-height dowel canopy. Computed bed shear stresses
621 in the uniform-height dowels were 3-5 times higher than those for the variable-height dowels,
622 and they spanned a much wider range than any of the other canopies did for a single density
623 (Figure 8). The much greater exposure of the bed in uniform-height canopies compared to
624 variable-height canopies follows naturally from the observations that (i) turbulence intensity
625 and Reynolds stresses in the canopy shear layer are much greater, and (ii) maximum
626 Reynolds stresses were observed closer to the bed, at $z \approx h_c$ instead of $z \approx 1.5h_c$ (Figure 3b,c).

627 Consequently, bed shear stresses in the uniform-height dowel canopy were up to two times
628 greater than would have been expected for a real pneumatophore canopy of similar density
629 (Figure 8), particularly for the deeper submerged canopies. Based on these observations we
630 can extend the findings by Liu et al. [35], who observed a reduction of the maximum
631 turbulence intensity in a double-layer canopy compared to a uniform-height canopy, to
632 natural heterogeneous vegetation canopies.
633
634 Previous experimental studies with idealized uniform-height canopies [e.g. 20, 22, 28, 55, 57]
635 may not provide appropriate results to directly infer sediment dynamics in natural aquatic
636 canopies that typically have a non-uniform height distribution. Likewise, turbulence-
637 resolving numerical model simulations often assume uniform vegetation properties, including
638 vegetation height [e.g. 12, 24, 52, 58, 59], thereby not accounting for the identified impacts of
639 heterogeneity in vegetation canopies on flow dynamics. Our findings suggest that a constant
640 scaling parameter of ~0.45 could be applied to the maximum friction velocity (scaled by the
641 free-stream velocity) for a uniform-height canopy to obtain a value representative of a natural
642 variable-height canopy, regardless of the canopy density and submergence (Figure 6b),
643 keeping in mind that at the same time this maximum translates from the top of the canopy (z
644 $\approx h_c$) to a height similar to the average plus the standard deviation of the canopy height ($z \approx$
645 $\mu(h_c) + \sigma(h_c)$). Following these modifications to the turbulent properties, a similar scaling
646 could be developed for near-bed turbulence intensities (c.f. Figure 5b) and bed shear stresses
647 (c.f. Figure 8) in natural canopies, but these relations would require further investigation to be
648 confirmed across a broader range of uniform-height dowel canopy densities.
649

5 Conclusions

Natural canopies of mangrove pneumatophores often exhibit a heterogeneous distribution with substantial variability in both height and diameter of vegetation elements [e.g. 37, 38]. Such heterogeneous natural canopies deviate significantly from the uniform dowel canopies that are frequently used in experiments to study flows in aquatic vegetation.

Heterogeneity of the canopy height was found to significantly reduce the strength of the canopy shear layer in comparison to a canopy with uniform height. Maximum friction velocities, scaled by the free-stream velocity, were two times greater over uniform-height dowel canopies in the present and previous studies than over a natural pneumatophore canopy or dowel mimics with a similar, natural height distribution. Apart from the reduced turbulence over the variable-height pneumatophores and dowels, the turbulence maxima were also observed to be shifted upward, at $z \approx 1.5\ h_c$ which equated to the mean plus the standard deviation of the height of the canopy elements, as opposed to at h_c for uniform-height dowel canopies. These two effects combined caused variable-height canopies to be less susceptible to enhanced near-bed turbulence levels. Turbulent stresses in the pneumatophore canopies were substantially lower and bed shear stresses were up to two times smaller in pneumatophore canopies compared to uniform-height dowel canopies with similar densities.

Conversely, the variability in height and shape in pneumatophore canopies were found to have a very limited impact on the vertical velocity distributions in vegetated flows, as did the spatial distribution of the vegetation elements. The ratio of the within-canopy velocity to the free-stream velocity above the canopies showed a monotonous decrease with an adjusted density parameter $\varphi(h/h_c)$ that incorporates the submergence ratio of the canopy. This trend

was confirmed across present and past experiments with real pneumatophores and vegetation mimics that covered a wide range of flow conditions and canopy arrangements.

The present findings demonstrate substantial differences in the hydrodynamics between canopies of real pneumatophores and dowel mimics, which may have significant implications for predictions of sediment transport and deposition within vegetated regions. Based on the observed reductions of maximum friction velocities and bed shear stresses in variable-height canopies, real pneumatophores may be much more efficient sediment traps than can be predicted based on uniform-height dowel experiments and model simulations.

Acknowledgements

This research is funded by the Royal Society of New Zealand's Marsden Fund (grant number 14-UOW-011). We thank Dean Sandwell for his help with setting up the flume experiments, and Carolyn Lundquist and Nicola Lovett for their help with the pneumatophore collection. We also thank two anonymous reviewers for their constructive feedback.

Notation

Commented [EH9]: As suggested by reviewer 1.

a	Frontal canopy density per unit area [m^{-1}]
C_D	Canopy element drag coefficient [-]
d	Canopy element diameter [m]
h	Water depth [m]
h_c	Canopy height [m]
k	Turbulent kinetic energy [m^2/s^2]
N	Canopy density [m^{-2}]
Re	Flow Reynolds number [-]
Re_d	Stem Reynolds number of the canopy [-]
u, v, w	Streamwise (x), spanwise (y) and vertical (z) velocities [m/s]
u', v', w'	Turbulent streamwise (x), spanwise (y) and vertical (z) velocities [m/s]
$u'w'$	Reynolds stress [m^2/s^2]
u_*	Friction velocity [m/s]
u_{*h_c}	Friction velocity at the top of the canopy $z = h_c$ [m/s]

u_{*max}	Maximum friction velocity over the full water depth h [m/s]
U	Free-stream velocity prior to canopy introduction [m/s]
U_c	Depth-averaged within-canopy velocity for $0 \leq z \leq h_c$ [m/s]
U_0	Depth-averaged plane bed velocity for $0 \leq z \leq h_c$ [m/s]
U_∞	Free-stream velocity (at $z = h$ - 0.05 m) [m/s]
z	Height above bed [m]
ΔU	Canopy vortex velocity scale U_∞-U_c [m/s]
ρ	Mass-density of water [kg/m^3]
τ_b	Bed shear stress [N/m^2]
$\tau_{b,0}$	Bed shear stress for plane bed without canopy [N/m^2]
φ	Cross-sectional canopy density [-]
$\varphi(h/h_c)$	Submergence-adjusted canopy density parameter [-]
$\overline{...}$	Temporally averaged variable
$\langle ... \rangle$	Spatially averaged variable

691

References

[1] Mazda Y, E Wolanski. Hydrodynamics and modeling of water in magnrove areas. in: GME Perillo, E Wolanski, DR Cahoon, MM Brinson, (Eds.). Coastal Wetlands: An integrated ecosystem approach. 1 ed. Elsevier2009. pp. 231-61.

[2] Nepf HM. Hydrodynamics of vegetated channels. Journal of Hydraulic Research. 50 (2012) 262-79, doi: http://doi.org/10.1080/00221686.2012.696559.

[3] Tempest JA, I Möller, T Spencer. A review of plant-flow interactions on salt marshes: the importance of vegetation structure and plant mechanical characteristics. Wiley Interdisciplinary Reviews: Water. 2 (2015) 669-81, doi: http://doi.org/10.1002/wat2.1103.

[4] Mullarney JC, SM Henderson. The effect of marine vegetation on shorelines. in: V Pan-chang, J Kaihatu, (Eds.). Advances in Coastal Hydraulics (in press). World Scientific Publishing Ltd.2017.

[5] King AT, RO Tinoco, EA Cowen. A k–ε turbulence model based on the scales of vertical shear and stem wakes valid for emergent and submerged vegetated flows. Journal of Fluid Mechanics. 701 (2012) 1-39, doi: http://doi.org/10.1017/jfm.2012.113.

[6] Yager EM, MW Schmeeckle. The influence of vegetation on turbulence and bed load transport. J Geophys Res. 118 (2013) 1585-601, doi: http://doi.org/10.1002/jgrf.20085.

[7] Ghisalberti M, H Nepf. Mass transport in vegetated shear flows. Environmental Fluid Mechanics. 5 (2005) 527-51, doi: http://doi.org/10.1007/s10652-005-0419-1.

[8] Marion A, V Nikora, S Puijalon, T Bouma, K Koll, F Ballio, et al. Aquatic interfaces: a hydrodynamic and ecological perspective. Journal of Hydraulic Research. 52 (2014) 744-58, doi: http://doi.org/10.1080/00221686.2014.968887.

[9] Zong L, H Nepf. Flow and deposition in and around a finite patch of vegetation. Geomorphology. 116 (2010) 363-72, doi: http://dx.doi.org/10.1016/j.geomorph.2009.11.020.

[10] Furukawa K, E Wolanski. Sedimentation in Mangrove Forests. Mangroves Salt Marshes. 1 (1996) 3-10, doi: http://doi.org/10.1023/a:1025973426404.

[11] Temmerman S, G Govers, S Wartel, P Meire. Spatial and temporal factors controlling short-term sedimentation in a salt and freshwater tidal marsh, scheldt estuary, Belgium, SW Netherlands. Earth Surface Processes and Landforms. 28 (2003) 739-55, doi: http://doi.org/10.1002/esp.495.

[12] Bouma TJ, LA Van Duren, S Temmerman, T Claverie, A Blanco-Garcia, T Ysebaert, et al. Spatial flow and sedimentation patterns within patches of epibenthic structures: Combining field, flume and modelling experiments. Cont Shelf Res. 27 (2007) 1020-45, doi: http://doi.org/10.1016/j.csr.2005.12.019.

[13] Ganthy F, L Soissons, P-G Sauriau, R Verney, A Sottolichio. Effects of short flexible seagrass Zostera noltei on flow, erosion and deposition processes determined using flume experiments. Sedimentology. 62 (2015) 997-1023, doi: http://doi.org/10.1111/sed.12170.

[14] van Maanen B, G Coco, KR Bryan. On the ecogeomorphological feedbacks that control tidal channel network evolution in a sandy mangrove setting. Proceedings of the Royal Society of London A: Mathematical, Physical and Engineering Sciences. 471 (2015) 1-24, doi: http://doi.org/10.1098/rspa.2015.0115.

[15] Young BM, EL Harvey. A Spatial Analysis of the Relationship Between Mangrove (Avicennia marina var. australasica) Physiognomy and Sediment Accretion in the Hauraki Plains, New Zealand. Estuar Coast Shelf Sci. 42 (1996) 231-46, doi: http://doi.org/10.1006/ecss.1996.0017.

[16] Krauss KW, JA Allen, DR Cahoon. Differential rates of vertical accretion and elevation change among aerial root types in Micronesian mangrove forests. Estuar Coast Shelf Sci. 56 (2003) 251-9, doi: http://doi.org/10.1016/s0272-7714(02)00184-1.

Formatted: English (New Zealand)

740 [17] Spenceley AP. The role of pneumatophores in sedimentary processes. Mar Geol. 24
741 (1977) M31-M7, doi: http://dx.doi.org/10.1016/0025-3227(77)90001-9.
742 [18] Mullarney JC, SM Henderson, BK Norris, KR Bryan, AT Fricke, DR Sandwell. A
743 question of scale: The role of turbulence within mangrove roots in shaping the Mekong Delta.
744 Oceanography (in press). (2017).
745 [19] Norris BK, JC Mullarney, KR Bryan, SM Henderson. The effect of pneumatophore
746 density on turbulence: a field study in a Sonneratia-dominated mangrove forest, Vietnam.
747 Continental Shelf Research (under review). (2017).
748 [20] Chen Z, C Jiang, H Nepf. Flow adjustment at the leading edge of a submerged aquatic
749 canopy. Water Resources Research. 49 (2013) 5537-51, doi:
750 http://doi.org/10.1002/wrcr.20403.
751 [21] Liu D, P Diplas, JD Fairbanks, CC Hodges. An experimental study of flow through rigid
752 vegetation. J Geophys Res. 113 (2008) F04015, doi: http://doi.org/10.1029/2008JF001042.
753 [22] Lowe RJ, JR Koseff, SG Monismith. Oscillatory flow through submerged canopies: 1.
754 Velocity structure. J Geophys Res. 110 (2005) C10016, doi:
755 http://doi.org/10.1029/2004JC002788.
756 [23] Dunn C, F Lopez, M Garcia. Mean flow and turbulence in a laboratory channel with
757 simulated vegetation. Hydraulic Engineering Series. University of Illinois, Urbana, Illinois,
758 1996. pp. 148.
759 [24] Murphy E, M Ghisalberti, HM Nepf. Model and laboratory study of dispersion in flows
760 with submerged vegetation. Water Resources Research. 43 (2007) W05438, doi:
761 http://doi.org/10.1029/2006wr005229.
762 [25] White BL, HM Nepf. Shear instability and coherent structures in shallow flow adjacent
763 to a porous layer. Journal of Fluid Mechanics. 593 (2007) 1-32, doi:
764 http://doi.org/10.1017/S0022112007008415.
765 [26] Tanino Y, HM Nepf. Lateral dispersion in random cylinder arrays at high Reynolds
766 number. Journal of Fluid Mechanics. 600 (2008) 339-71, doi:
767 http://doi.org/10.1017/S0022112008000505.
768 [27] Nepf HM. Drag, turbulence, and diffusion in flow through emergent vegetation. Water
769 Resources Research. 35 (1999) 479-89, doi: http://doi.org/10.1029/1998wr900069.
770 [28] Nepf HM, M Ghisalberti, B White, E Murphy. Retention time and dispersion associated
771 with submerged aquatic canopies. Water Resources Research. 43 (2007) W04422, doi:
772 http://doi.org/10.1029/2006wr005362.
773 [29] Nepf HM, ER Vivoni. Flow structure in depth-limited, vegetated flow. J Geophys Res.
774 105 (2000) 28547-57, doi: http://doi.org/10.1029/2000jc900145.
775 [30] Raupach MR, JJ Finnigan, Y Brunet. Coherent Eddies and Turbulence in Vegetation
776 Canopies: The Mixing-Layer Analogy. Boundary-Layer Meteorology. 78 (1996) 351-82, doi:
777 http://doi.org/10.1007/978-94-017-0944-6_15.
778 [31] Ghisalberti M, HM Nepf. Mixing layers and coherent structures in vegetated aquatic
779 flows. Journal of Geophysical Research: Oceans. 107 (2002) 3-1-3-11.
780 [32] Sukhodolova TA, AN Sukhodolov. Vegetated mixing layer around a finite-size patch of
781 submerged plants: 1. Theory and field experiments. Water Resources Research. 48 (2012)
782 W10533, doi: http://doi.org/10.1029/2011WR011804.
783 [33] Lacy JR, S Wyllie-Echeverria. The influence of current speed and vegetation density on
784 flow structure in two macrotidal eelgrass canopies. Limnol Oceanogr. 1 (2011) 38-55, doi:
785 http://doi.org/10.1215/21573698-1152489.
786 [34] Järvelä J. Flow resistance of flexible and stiff vegetation: a flume study with natural
787 plants. Journal of Hydrology. 269 (2002) 44-54, doi: http://doi.org/10.1016/S0022-
788 1694(02)00193-2.

789 [35] Liu D, P Diplas, CC Hodges, JD Fairbanks. Hydrodynamics of flow through double
790 layer rigid vegetation. Geomorphology. 116 (2010) 286-96, doi:
791 http://dx.doi.org/10.1016/j.geomorph.2009.11.024.
792 [36] Tomlinson PB. The botany of mangroves. Cambridge University Press, Cambridge, UK,
793 1986.
794 [37] Horstman EM, CM Dohmen-Janssen, PMF Narra, NJF Van den Berg, M Siemerink,
795 SJMH Hulscher. Wave attenuation in mangroves: A quantitative approach to field
796 observations. Coastal Engineering. 94 (2014) 47-62, doi:
797 http://doi.org/10.1016/j.coastaleng.2014.08.005.
798 [38] Liénard J, K Lynn, N Strigul, BK Norris, D Gatziolis, JC Mullarney, et al. Efficient
799 three-dimensional reconstruction of aquatic vegetation geometry: Estimating morphological
800 parameters influencing hydrodynamic drag. Estuar Coast Shelf Sci. 178 (2016) 77-85, doi:
801 http://dx.doi.org/10.1016/j.ecss.2016.05.011.
802 [39] Horstman EM, KR Bryan, JC Mullarney, CA Pilditch. Model versus nature:
803 hydrodynamics in mangrove pneumatophores. in: P Lynett, (Ed.). Proceedings of 35th
804 Conference on Coastal Engineering. 2017-05-12 ed. Coastal Engineering Research Council,
805 Antalya, Turkey, 2016.
806 [40] Miller DC, A Norkko, CA Pilditch. Influence of diet on dispersal of horse mussel Atrina
807 zelandica biodeposits. Mar Ecol Prog Ser. 242 (2002) 153-67, doi:
808 http://doi.org/10.3354/meps242153.
809 [41] Horstman EM, CM Dohmen-Janssen, SJMH Hulscher. Flow routing in mangrove
810 forests: A field study in Trang province, Thailand. Cont Shelf Res. 71 (2013) 52-67, doi:
811 http://doi.org/10.1016/j.csr.2013.10.002.
812 [42] Bryan KR, W Nardin, JC Mullarney, S Fagherazzi. The role of cross-shore tidal
813 dynamics in controlling intertidal sediment exchange in mangroves in Cù Lao Dung,
814 Vietnam. Cont Shelf Res. 147 (2017) 128-43, doi: https://doi.org/10.1016/j.csr.2017.06.014.
815 [43] Rusello PJ, A Lohrmann, E Siegel, T Maddux. Improvements in acoustic doppler
816 velocimetery. The 7th Int Conf on Hydroscience and Engineering. ICHE, Philadelphia, USA,
817 2006. pp. 1-16.
818 [44] Hurther D, U Lemmin. A Correction Method for Turbulence Measurements with a 3D
819 Acoustic Doppler Velocity Profiler. Journal of Atmospheric and Oceanic Technology. 18
820 (2001) 446-58, doi: http://doi.org/10.1175/1520-0426(2001)018<0446:acmftm>2.0.co;2.
821 [45] Brand A, C Noss, C Dinkel, M Holzner. High-Resolution Measurements of Turbulent
822 Flow Close to the Sediment–Water Interface Using a Bistatic Acoustic Profiler. Journal of
823 Atmospheric and Oceanic Technology. 33 (2016) 769-88, doi: http://doi.org/10.1175/JTECH-
824 D-15-0152.1.
825 [46] Raupach MR, RH Shaw. Averaging procedures for flow within vegetation canopies.
826 Boundary-Layer Meteorology. 22 (1982) 79-90, doi: http://doi.org/10.1007/bf00128057.
827 [47] Nortek. Vectrino-II profiling velocimeter User Guide. Halifax, Canada, 2011. pp. 37.
828 [48] Van Rijn LC. Principles of fluid flow and surface waves in rivers, estuaries, seas and
829 oceans. Aqua Publications, The Netherlands, 2008.
830 [49] Leonard LA, ME Luther. Flow hydrodynamics in tidal marsh canopies. Limnol
831 Oceanogr. 40 (1995) 1474-84, doi: http://doi.org/10.4319/lo.1995.40.8.1474.
832 [50] Stoesser T, SJ Kim, P Diplas. Turbulent Flow through Idealized Emergent Vegetation.
833 Journal of Hydraulic Engineering. 136 (2010) 1003-17, doi:
834 http://doi.org/10.1061/(ASCE)HY.1943-7900.0000153.
835 [51] Ghisalberti M, HM Nepf. The limited growth of vegetated shear layers. Water Resources
836 Research. 40 (2004) W07502, doi: http://doi.org/10.1029/2003WR002776.

[52] Poggi D, A Porporato, L Ridolfi, JD Albertson, GG Katul. The Effect of Vegetation Density on Canopy Sub-Layer Turbulence. Boundary-Layer Meteorology. 111 (2004) 565-87, doi: http://doi.org/10.1023/B:BOUN.0000016576.05621.73.
[53] Naden P, P Rameshwaran, O Mountford, C Robertson. The influence of macrophyte growth, typical of eutrophic conditions, on river flow velocities and turbulence production. Hydrological Processes. 20 (2006) 3915-38, doi: http://doi.org/10.1002/hyp.6165.
[54] Nepf HM. Flow and Transport in Regions with Aquatic Vegetation. Annual Review of Fluid Mechanics. 44 (2012) 123-42, doi: http://doi.org/10.1146/annurev-fluid-120710-101048.
[55] Tinoco RO, G Coco. A laboratory study on sediment resuspension within arrays of rigid cylinders. Advances in Water Resources. 92 (2016) 1-9, doi: http://dx.doi.org/10.1016/j.advwatres.2016.04.003.
[56] Hansen JCR, MA Reidenbach. Wave and tidally driven flows in eelgrass beds and their effect on sediment suspension. Mar Ecol Prog Ser. 448 (2012) 271-87, doi: http://doi.org/10.3354/meps09225.
[57] Le Bouteiller C, JG Venditti. Sediment transport and shear stress partitioning in a vegetated flow. Water Resources Research. 51 (2015) 2901-22, doi: http://doi.org/10.1002/2014WR015825.
[58] López F, M García. Mean flow and turbulence structure of open-channel flow through non-emergent vegetation. Journal of Hydraulic Engineering. 127 (2001) 392-402, doi: http://dx.doi.org/10.1061/(ASCE)0733-9429(2001)127:5(392).
[59] Defina A, AC Bixio. Mean flow and turbulence in vegetated open channel flow. Water Resources Research. 41 (2005) 1-12, doi: http://doi.org/10.1029/2004WR003475.

6 Supplementary material

Density effects in real pneumatophore canopies

This supplement presents the results of the experiments with the different pneumatophore densities (Pneum-LD, Pneum-AD, Pneum-HD; see Table 2). Significant reductions of the within-canopy flow velocities were observed for all three densities of the real pneumatophore canopies, compared to the plane bed scenario, accompanied by enhanced over-canopy flow (Figure 9a). Velocity reductions occurred for $z \lesssim 2h_c$, above which faster flow velocities were observed compared to the plane bed scenario. For the experiments with 0.30 m water depth, the ratios of the within-canopy velocity to the free-stream velocity decreased from U_c/U_∞ = 0.46 for the lowest pneumatophore density, to 0.37 for the average density pneumatophore cover and 0.27 for the highest pneumatophore density (Table 2). For comparison, for the plane bed scenario with h = 0.30 m, the ratio of the depth-averaged velocity over the equivalent canopy height compared to the free-stream velocity U_0/U_∞ was 0.67.

Turbulence generation in the canopy shear layer increased with the velocity gradient across the top of the canopy and hence with the pneumatophore density, in agreement with previous observations by e.g. Dunn et al. (1996). Conversely, the near-bed Reynolds stresses at z = 0.015 m ($z = 0.2h_c$) decreased with vegetation density, by up to 22% and 63% (compared to the low pneumatophore density) for the average and high densities, respectively, owing to the lower within-canopy velocities (Figure 9c).

The velocity profiles for each canopy densities, scaled by the velocity at the top of the canopy, collapsed for the three water depths and two flow rates (Figure 9d), similar to the results presented in Figure 3g. The profiles of the turbulence intensity and the normalized

Reynolds' stresses were similar for experiments with different flow rates, but did not collapse for the different water depths (Figure 9h,i).

The amplification of within-canopy turbulence with a reduction of the canopy submergence (Figure 3e) became more pronounced with an increase in canopy density. Near-bed (z/h_c = 0.2) turbulent kinetic energy at the shallowest water depth was up to 25%, 72% and 166% larger than for the deepest submergence, for the lowest, average and highest pneumatophore densities, respectively. Similarly, the near-bed Reynolds stresses increased up to 18%, 38% and 61% for the low, average and high pneumatophore densities, respectively, between the deepest and the shallowest canopy submergence.

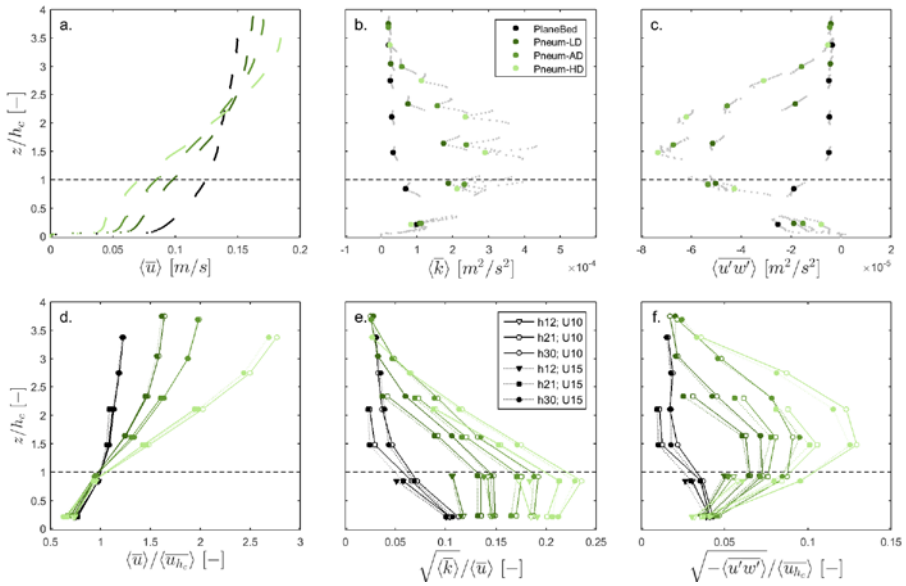

Figure 9 – Combined results of the flume experiments for all pneumatophore canopies. Spatially-averaged vertical profiles of (a) streamwise velocity, (b) turbulent kinetic energy, and (c) Reynolds stress, for all vegetation densities at 0.30 m water depth and the high flow rate (0.15 m/s). ~~*(d-f) Show the same as (a-c) for the greatest pneumatophore density and high flow rate (U = 0.15 m/s) at multiple water depths.*~~ *Spatially-averaged vertical profiles of (~~g~~d) streamwise velocity scaled by the velocity at the top of the canopy, (~~h~~e) turbulence intensity, and (~~i~~f) friction velocity scaled by the velocity at the top of the*

canopy, for all canopy densities (different colours as in a-c), at all water depths and at both flow rates. Dashed horizontal black lines indicate the average canopy height. Panels (b,c), ~~e and f~~ present the reliable turbulence observations from the sweet spots (solid symbols) and the noise-affected observations throughout the remainder of the observed profiles (grey dots; see text for details). Legend key: canopy types as in Table 1; h12/h21/h30 = 0.12/0.21/0.30 m water depth; U10/U15 = low/high flow rate comparing to a free-stream velocity of 0.10/0.15 m/s over the plane bed.